

# Topological Aspects of Dirac Fermions in a Kagomé Lattice

Xinyuan Zhou<sup>1,2,\*</sup> and Hua Chen<sup>1,2,\*</sup>

<sup>1</sup>Department of Physics, Zhejiang Normal University, Jinhua 321004, China

<sup>2</sup>Zhejiang Institute of Photoelectronics & Zhejiang Institute for Advanced Light Source, Zhejiang Normal University, Jinhua 321004, China

(Dated: December 6, 2024)

The Dirac fermion with linear dispersion in the kagomé lattice governs the low-energy physics of different valleys at two inequivalent corners of hexagonal Brillouin zone. The effective Hamiltonian based on the cyclic permutation symmetry of sublattices is constructed to show that the topology of Dirac fermions at these two valleys is characterized by opposite winding numbers. For spinless fermions, the Dirac semimetal phase is unstable against the many-particle interactions due to the intervalley scattering, which spontaneously breaks the translation symmetry. The Dirac fermions acquire a mass term from the simultaneous charge and bond orderings. In this phase, the developed bond texture underlies a hollow-star-of-David pattern in a tripled Wigner-Seitz cell of kagomé lattice. It is further demonstrated that the twisting of Dirac mass with vorticity leads to zero Dirac modes at the vortex core, which are intimately related to the fractionalization. The hollow-star-of-David phase is shown to have a distinct  $\mathbb{Z}_6$  Berry phase with its sign-change counterpart of Dirac mass, *i.e.* the hexagonal phase, shedding light on the topological origin of zero Dirac modes around the vortex core.

The kagomé lattice with diverse quantum phenomena [1] holds promise to study the interplay between geometry, topology and correlation for its typical features in band structures, including Dirac points [2–11], quadratic band crossings [12–16], van Hove singularities [17–26], as well as flat bands [27–33]. In particular, Dirac semimetals (DSMs) with linear dispersion are usually believed as a precursor of various topological insulating states [34, 35]. The routine recipe for realizing topological insulators from DSMs is the inclusion of spin-orbit couplings, which can be traced back to the studies in graphene [36, 37]. In kagomé lattices, the intrinsic spin-orbit coupling preserving time-reversal symmetry opens a gap at Dirac points, giving rise to quantum spin Hall insulators with  $\mathbb{Z}_2$  topology [38–40]. In addition, the ferromagnetic ordering breaking time-reversal symmetry further drives a staggered magnetic flux phase, rendering quantum anomalous Hall insulators with nontrivial Chern numbers [8, 41]. Moreover, an alternative recipe is the spatial distortion away from the ideal kagomé lattice. The second-order topological insulators are theoretically proposed in the breathing kagomé lattice [42–46]. The topologically protected corner states are experimentally detected in artificial systems, including acoustic systems [47] and photonic waveguides [48, 49]. Besides topological insulators, another issue of topological relevance is the zero Dirac modes (ZDMs) at vortex defects [50–53], which are predicted in a Kekulé distortion of honeycomb lattices [54–56] and lead to fractionalization and anyon statistics [57–60]. However, comprehensive understanding of ZDMs is still missing for kagomé lattices. In this work, we show that the Dirac fermions acquire a mass in a distorted kagomé lattice with the bond orders of hollow-star-of-David (HSD) pattern driven by many-particle interactions. Notably, the charge density wave of star-of-David pattern at van Hove singularities is un-

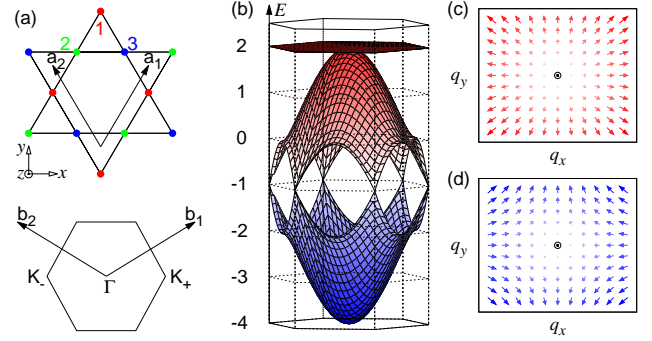


FIG. 1. (a) Kagomé lattice is a triangular Bravais lattice with three sublattices in a unit cell and the corresponding hexagonal Brillouin zone in reciprocal space. (b) The band structure of tight-binding model in Eq. (1) with nearest-neighbor hopping  $t = 1$ . The pseudovector field  $\mathbf{p} \equiv (p_x, p_y)$  near the Dirac point at the corner of hexagonal Brillouin zone  $K_+$  (c) and  $K_-$  (d) with the winding number  $\mathcal{W} = \pm 1$  in Eq. (4) resembles the vortex in XY systems.

covered in kagomé materials [61, 62]. Twisting the mass of Dirac fermions by a vortex gives rise to ZDMs, that are universal with the Majorana bound states in topological superconductors [63]. It is further demonstrated that the HSD phase and its sign-change-of-mass counterpart hexagonal phase can be topologically distinguished by  $\mathbb{Z}_6$  Berry phase. Bound states at the interface between domains governed by distinct topological invariants are topologically protected, thereby revealing the topological origin of ZDMs around the vortex core.

We begin with the tight-binding model

$$H_{\text{TB}} = -t \sum_{\langle ij \rangle} c_i^\dagger c_j \quad (1)$$

that describes the nearest-neighbor hopping processes of

spinless fermions in the kagomé lattice, as depicted in Fig. 1(a). Here,  $t$  is the hopping integral,  $c_i$  and  $c_i^\dagger$  are the annihilation and creation field operators at  $i$ th site, respectively. Introducing a spinor representation of three sublattices  $c_{\mathbf{k}} = [c_{1\mathbf{k}}, c_{2\mathbf{k}}, c_{3\mathbf{k}}]^T$ , the Bloch Hamiltonian with the unit-cell gauge in reciprocal space reads

$$\mathcal{H}_{\mathbf{k}} = \begin{bmatrix} 0 & 1 + \exp[ik_1] & 1 + \exp[ik_2] \\ 1 + \exp[-ik_1] & 0 & 1 + \exp[ik_3] \\ 1 + \exp[-ik_2] & 1 + \exp[-ik_3] & 0 \end{bmatrix} \quad (2)$$

with the crystal momenta  $k_{i=1,2,3} = \mathbf{k} \cdot \mathbf{a}_i$  being expressed in terms of the primitive lattice vectors  $\{\mathbf{a}_1, \mathbf{a}_2, \mathbf{a}_3 \equiv -\mathbf{a}_1 + \mathbf{a}_2\}$  respectively. The band structure of the tight-binding model in Eq. (1) is plotted in Fig. 1(b). Notably, the highest band is a perfectly flat band with a quadratic band touching at  $\Gamma$  point and the lowest two bands cross at the corners  $K_{\pm}$  points of hexagonal Brillouin zone (HBZ). Moreover, the Bloch Hamiltonian  $\mathcal{H}_{\mathbf{k}}$  in Eq. (2) at  $K_{\pm}$  points is left invariant under the cyclic permutation of three sublattices. Therefore, the corresponding Bloch states are characterized by the irreducible representations of group  $C_3$ . To describe the corresponding low-energy behavior around  $K_{\pm}$  points, we further derive the effective  $k \cdot p$  model

$$\mathcal{H}_{K_{\pm}}(\mathbf{q}) = p_0\tau_0 + p_x\tau_x + p_y\tau_y + \mathcal{O}(q^2) \quad (3)$$

with the coefficients  $p_0 = -t$  and  $\{p_x, p_y\} = \sqrt{3}t\{\pm q_x, q_y\}$ . Here,  $\tau_0$  and  $\boldsymbol{\tau}$  are the identity matrix and Pauli matrices, respectively, operating on the space spanned by the irreducible representations  $E$  and  $A$  of group  $C_3$ . Diagonalizing  $\mathcal{H}_{K_{\pm}}(\mathbf{q})$  in Eq. (3) yields two isotropic bands  $E_{K_{\pm}}^{\pm}(\mathbf{q}) = -t \pm \sqrt{3}t|\mathbf{q}|$ , resulting in a linear dispersed Dirac cone with Fermi velocity  $v_F = \sqrt{3}t/\hbar$ . The pseudovector fields  $\mathbf{p} \equiv (p_x, p_y)$  around  $K_{\pm}$  points, shown in Figs. 1(c) and 1(d) respectively, have a  $p$ -wave symmetry. The topological charge of Dirac point is given by the winding number of pseudovector field

$$\mathcal{W} = \frac{1}{2\pi} \oint_{\mathcal{C}} \nabla\theta(\mathbf{q}) \cdot d\mathbf{q} = \pm 1 \quad (4)$$

for the  $K_{\pm}$  point respectively, where  $\theta \equiv \arctan(p_y/p_x)$  and  $\mathcal{C}$  is a contour enclosing the singular  $K_{\pm}$  points, indicating that the Dirac point carries a  $\pm\pi$  Berry flux.

Having established the single-particle physics, we are then in a position to study the effects of many-particle interactions. The interacting Hamiltonian of spinless fermions described by the inter-site interaction can be decoupled at the Hartree-Fock mean-field level

$$H_{\text{I}} = V \sum_{\langle ij \rangle} \left( n_i c_j^\dagger c_j + n_j c_i^\dagger c_i - n_i n_j - \chi_{ij} c_j^\dagger c_i - \chi_{ji} c_i^\dagger c_j + |\chi_{ij}|^2 \right), \quad (5)$$

where  $n_i = \langle c_i^\dagger c_i \rangle$  and  $\chi_{ij} = \langle c_i^\dagger c_j \rangle$  are the charge and bond mean-field order parameters, respectively. The

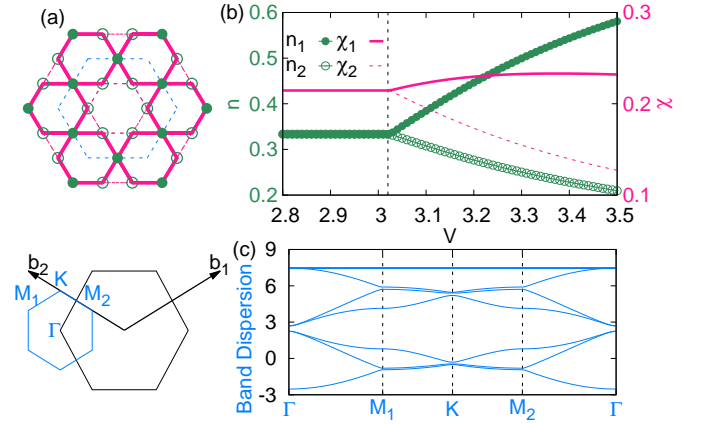


FIG. 2. (a) The pictorial representation of charge and bond patterns for the hollow-star-of-David insulator phase in an enlarged Wigner-Seitz unit cell indicated by blue dash lines, and the corresponding reduced (original) hexagonal Brillouin zone indicated by blue (black) lines in reciprocal space. (b) The evolution of self-consistent mean-field order parameters including the charge density  $n$  with filled (open) circles indicating large (small) local on-site charge, as well as the bond order  $\chi$  with solid (dash) lines indicating strengthened (weakened) inter-site bond hopping renormalizations, as a function of inter-site interactions  $V$  at near-neighbor hopping  $t = 1$ . The black dashed line at  $V_c$  marks the phase transition between Dirac semimetal phase and hollow-star-of-David insulator phase with its charge and bond patterns in (a). (c) The band structure along high-symmetry paths in Brillouin zone at  $\{t, V\} = \{1, 3.1\}$ .

charge  $n$  related terms in Eq. (5) promote charge density waves, and the bond  $\chi$  related ones renormalize the hopping integral  $t$  in tight-binding Hamiltonian Eq. (1) by lowering the ground-state energy. Before proceeding, it is instructive to discuss the many-particle instability from the weak-coupling limit with the Fermi energy being pinned at Dirac points. The single-particle Bloch states around the corners  $K_{\pm}$  points of HBZ are characterized by Dirac fermions at two inequivalent valleys. The many-particle interactions may scatter the Dirac fermions via the intra and inter valley processes. For the latter, the umklapp scattering between the corners of HBZ transfers a lattice phonon which carries the momentum of multiple primitive reciprocal vectors. This process folds two  $K_{\pm}$  points to  $\Gamma$  point and underlies the reduced HBZ (RHBZ), accompanied by the tripling of Wigner-Seitz cell in Kagomé lattices, as illustrated by the blue dash lines in Fig. 1(a). The  $\sqrt{3} \times \sqrt{3}$  ordered states are theoretically predicted at first [2] and experimentally discovered later [64, 65]. Besides, the inter valley coherent phase is extensively studied in the context of twisted bilayer graphene [66–69]. In our numerical calculations, the order parameters in both the charge  $n$  and bond  $\chi$  channels are self-consistently determined. Figure 2(b) shows the evolution of order parameters as a function

of inter-site interaction  $V$  at hopping integral  $t = 1$ . A critical interaction  $V_c \approx 3.02$  is found to separate DSM phase and hollow-star-of-David insulator (HSDI) phase. The HSDI phase, which is essentially driven by the inter valley scattering process, spontaneously breaks the translation symmetry of kagomé lattice with its charge and bond pattern sketched in Fig. 2(a). The strengthened bonds renormalized by real-valued order parameters  $\chi$  in an enlarged Wigner-Seitz unit cell highlight a HSD pattern with its vertices being composed of large on-site charge  $n$ . In contrast, the complex-valued bond orders at the van Hove singularities breaks time reversal symmetry with spontaneous loop currents [70, 71]. To facilitate our understanding on the low-energy physics, we next derive the effective Hamiltonian in the vicinity of Dirac points  $K_{\pm}$  by projecting the mean-field Hamiltonian in Eq. (5) onto the irreducible representations of group  $C_3$  through a perturbative treatment. Introducing a pseudospin  $\sigma_z = \pm 1$  to label the valley degree of freedom at  $K_{\pm}$  points, the resulting Hamiltonian takes the following form

$$\mathcal{H}_I = \sqrt{3}\delta t (q_x \tau_x \sigma_z + q_y \tau_y) + \Delta \tau_x \sigma_x \quad (6)$$

with  $\delta t = \frac{V}{2} (\chi_+ + \frac{\chi_-}{3})$  and  $\Delta = \frac{V}{3} (n_- - 2\chi_-)$  being expressed in terms of charge  $n_{\pm} = n_1 \pm n_2$  and bond  $\chi_{\pm} = \chi_1 \pm \chi_2$  order parameters. In Eq. (6), we have dropped the renormalization of Fermi energy, which is irrelevant to the low-energy physics. The bond orders of HSD pattern in the first term of Eq. (6) equally renormalize the Fermi velocity  $v_F = \sqrt{3} (t + \delta t) / \hbar$  of Dirac fermions at  $K_{\pm}$  points. Interestingly, the Dirac fermions, acquiring a mass term described by the charge and bond orders in the second term of Eq. (6), become gapped by the inter valley scattering. The band structure along high-symmetry paths of RHBZ in Fig. 2(c) is numerically calculated to confirm the insulating gap at the center  $\Gamma$  point of RHBZ in HSDI phase.

Having settled the nature of HSDI phase, we then study ZDMs in the presence of a vortex, which is intimately related to the fractionalization for its topological origin. To this end, we generalize the mass term  $\Delta$  in Eq. (6) with spatial dependence by focusing on the following Hamiltonian

$$\mathcal{H}_V = \hbar v_F (\hat{q}_x \tau_x \sigma_z + \hat{q}_y \tau_y) + (\Delta_{\ell}(\mathbf{r}) \sigma_+ + \Delta_{\ell}^*(\mathbf{r}) \sigma_-) \tau_x, \quad (7)$$

where the vortex potential  $\Delta_{\ell}(\mathbf{r}) = \Delta(r) \exp[i\ell\theta]$  in polar coordinates  $\mathbf{r} = (r, \theta)$  has vorticity  $\ell$  and Pauli matrices  $\sigma_{\pm} = \frac{1}{2}(\sigma_x \pm i\sigma_y)$ . Crucially, the bond orders in the mass term  $\Delta$  of Eq. (6) can be twisted as the complex-valued Dirac mass around the vortex core [4, 13]. It is easy to verify that the Hamiltonian in Eq. (7) commutes with the following total angular momentum operator

$$J_z = L_z + \frac{\hbar}{2} \sigma_z (\tau_z - \ell) \quad (8)$$

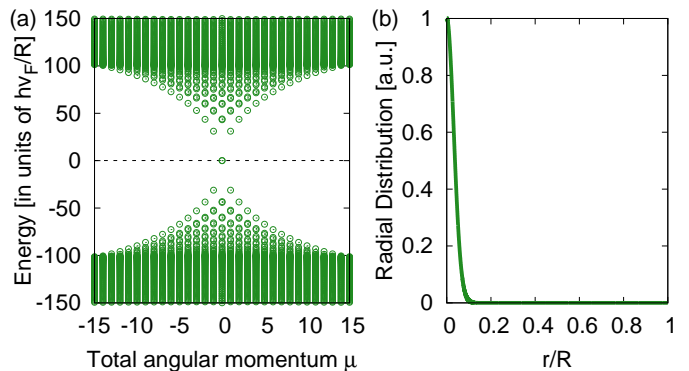


FIG. 3. (a) The energy spectrum of Dirac fermions immersed in a vortex  $\Delta_{\ell=-1}(\mathbf{r}) = \Delta(r) \exp[-i\theta]$  with  $\Delta(r) = \Delta \tanh(r/\xi)$  as a function of the eigenvalue  $\mu$  of total angular momentum operator in Eq. (8). The strength and size of vortex core are set as  $\Delta = 100\hbar v_F/R$  and  $\xi = R/5$ , respectively. In practical implement of numerical calculations, the number of zeros of the Bessel function  $N = 500$  is chosen to ensure the convergence of the low-energy spectrum. (b) The radial distribution of the zero Dirac mode localized at vortex core with total angular momentum  $\mu = 0$ .

where  $L_z = -i\hbar\partial_{\theta}$  is the orbital angular momentum. Consequently, the Hamiltonian shares the same eigenstates with the total angular momentum operator. The eigenstates for polar angle  $\theta$  can be labeled by the eigenvalue  $\mu$  of operator  $J_z$ . The radial eigenstates of the Hamiltonian can be numerically solved through the Bessel-Fourier transformation on a disk geometry with the principal quantum number  $E$  labeling the energy level. This numerical method is widely used to solve the Bogoliubov-de Gennes equation ever since the study of superconductivity [72]. The Hilbert space is spanned by a set of renormalized orthogonal bases

$$\phi_{j,\ell}(r) = \frac{\sqrt{2}}{R J_{\ell+1}(x_{j\ell})} J_{\ell}\left(x_{j\ell} \frac{r}{R}\right) \quad (9)$$

with  $x_{j\ell}$  denoting the  $j$ th zero of the Bessel function  $J_{\ell}(x)$ , which imposes the Dirichlet boundary condition at maximum radius  $R$  of the disk geometry. Expanding the space of valley pseudospin  $\sigma$ , the Hamiltonian in subspace labeled by the eigenvalue  $\mu$  of operator  $J_z$  reduces to the following matrix

$$\mathcal{H}_V^{\mu} = \begin{bmatrix} \hbar v_F q_- & \Delta_+ \\ \Delta_- & \hbar v_F q_+ \end{bmatrix}_{\sigma} \tau_+ + \begin{bmatrix} \hbar v_F q_-^{\dagger} & \Delta_-^{\dagger} \\ \Delta_+^{\dagger} & \hbar v_F q_+^{\dagger} \end{bmatrix}_{\sigma} \tau_- \quad (10)$$

where Pauli matrix  $\tau_{\pm} = \frac{1}{2}(\tau_x \pm i\tau_y)$ , the corresponding matrix elements  $q_{\pm}^{jj'} = \int dr r \phi_{j,\mu \mp \frac{\ell-1}{2}} \hat{q}_{\pm} \phi_{j',\mu \mp \frac{\ell+1}{2}}$ , and  $\Delta_{\pm}^{jj'} = \int dr r \phi_{j,\mu \pm \frac{\ell-1}{2}} \Delta(r) \phi_{j',\mu \mp \frac{\ell+1}{2}}$ . The calculated energy spectrum, shown in Fig. 3(a), is obtained via the diagonalization of the Hamiltonian matrix. In numerical calculations, the vortex is described by  $\Delta_{\ell=-1}(\mathbf{r}) =$

$\Delta \tanh(r/\xi) \exp[-i\theta]$  with  $\Delta$  and  $\xi$  characterizing the strength and size of vortex core, respectively. The spectrum above the gap  $|E| > \Delta$  is essentially continuous with the states being described by plane waves, but is actually discrete due to the quantum confinement of a finite disk. In contrast, the states below the gap  $|E| < \Delta$  are bound states in nature with a discrete spectrum, for which the Dirac fermions are confined by its mass term [73]. Of most significance are the bound midgap states with total angular momentum  $\mu = 0$  at zero energy. The ZDMs can be further identified through the analytical solutions of the Schrödinger equation with its Hamiltonian in Eq. (7). The linearly independent wave functions of these states up to an overall renormalization factor for generic vortex potentials are described by

$$|\pm\rangle = e^{\pm \frac{1}{\hbar v_F} \int^r \Delta(r') dr'} |\boldsymbol{\tau} = -\hat{z}, \boldsymbol{\sigma} = \pm \hat{y}\rangle \quad (11)$$

where Dirac notion  $|\boldsymbol{\tau}, \boldsymbol{\sigma}\rangle$  is the tensor product of pseudospin space. The ZDMs for vorticity  $\ell = +1$  are given by reversing the pseudospin direction  $\boldsymbol{\tau} = +\hat{z}$  in Eq. (11). The ZDM  $|+\rangle$  bounded near  $r = R$  can be regarded as the chiral edge state of topological insulators with time-reversal symmetry breaking by the vortex. In contrast, the other ZDM  $|-\rangle$  is bounded at the vortex core with its mechanism explored below. Unfortunately, direct comparisons between analytical and numerical solutions are unavailable because of different boundary conditions. Numerically, the ZDMs can be distinguished on application of a radial electric field by splitting the degeneracy. Figure 3(b) plots the radial distribution of the ZDM localized at the vortex core. Interestingly, a unitary transformation  $U = (\sigma_+ + \sigma_- \tau_x) \sigma_x$  on the Hamiltonian in Eq. (7) yields the effective Hamiltonian in describing the proximity induced superconductivity on the surface of topological insulators, which supports single Majorana bound state at the vortex core [63].

The effective low-energy Hamiltonian in Eq. (7) is universal in describing the physics of zero-energy bound states at the vortex core. In order to precisely pin down the topological origin of ZDMs, we further investigate  $\mathbb{Z}_6$  Berry phase with the tight-binding model, which is unique to the Kagomé lattice. To proceed, a local twist phase of hopping integrals on a hexagonal plaquette, as shown in Fig. 4(a), is first introduced under the constraint  $\sum_{i=1}^6 \theta_i = 0$ . The parameter space can be expressed as  $\boldsymbol{\Theta} = \sum_{i=1}^5 \theta_i \mathbf{e}_i$  in terms of five independent parameters with  $\mathbf{e}_i$  being orthogonal unit bases. The  $\mathbb{Z}_6$  Berry phase is then defined as a contour integral

$$\gamma = \int_{L_i} \mathcal{A}(\boldsymbol{\Theta}) \cdot d\boldsymbol{\Theta} \text{ mod } 2\pi \quad (12)$$

with  $\mathcal{A}(\boldsymbol{\Theta}) = -i \langle \psi(\boldsymbol{\Theta}) | \nabla_{\boldsymbol{\Theta}} | \psi(\boldsymbol{\Theta}) \rangle$  being the Berry connection [74]. The path  $L_i$  in  $\boldsymbol{\Theta}$  parameter space is defined as  $\mathbf{E}_{i-1} \rightarrow \mathbf{G} \rightarrow \mathbf{E}_i$  with  $\mathbf{E}_{i-1-5} = 2\pi \mathbf{e}_i$ ,

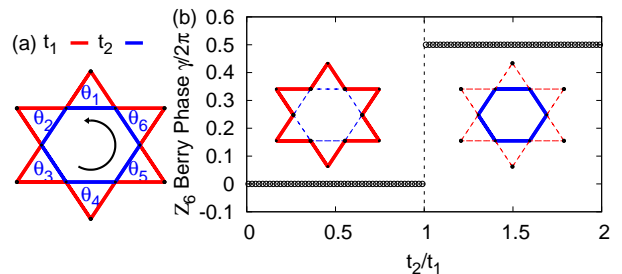


FIG. 4. (a) Schematic picture for the local twist phase of hopping integral on a hexagonal plaquette. (b) The  $\mathbb{Z}_6$  Berry phase  $\gamma$  in Eq. (12) as a function of the ratio of hopping integrals  $t_2/t_1$ . The bond textures (insert) for  $t_2/t_1 < 1$  and  $t_2/t_1 > 1$  regimes correspond the hollow-star-of-David and hexagonal patterns, respectively. These patterns are separated by the critical phase of Dirac semimetals marked by the dash line at  $t_1 = t_2$ . The numerical calculation is performed on a 1323-site cluster of hexagonal shape.

$\mathbf{E}_6 = \mathbf{E}_0 = \mathbf{0}$ , and  $\mathbf{G} = 1/6 \sum_{i=1}^6 \mathbf{E}_i$ . The  $\mathbb{Z}_6$  symmetry along path  $L_i$  guarantees the quantization of Berry phase  $\gamma = 2\pi\mathbb{Z}/6$  with  $\mathbb{Z}$  being an integer. As shown in Fig. 4(b), the  $\mathbb{Z}_6$  Berry phase  $\gamma = 0$  and  $\pi$  for HSD ( $t_1 > t_2$ ) and hexagonal ( $t_1 < t_2$ ) bond textures, respectively. These two insulating phase with distinct topological invariants are separated by the critical phase of DSMs at  $t_1 = t_2$ . Across the critical phase, the effective mass of Dirac fermions, c.f.  $\Delta$  in Eq. (6), changes its sign between HSD ( $\Delta > 0$ ) and hexagonal patterns ( $\Delta < 0$ ), accompanied by the close and reopen of the energy gap at the Dirac point. Such a sign change of Dirac mass terms is involved for  $|\ell|$  times as the polar angle changes from  $\theta = 0$  to  $2\pi$  in the vortex potential  $\Delta_\ell(\mathbf{r})$  of Eq. (7), resulting the topologically protected bound states of total number  $|\ell|$  in the vicinity of vortex core. These topologically protected states are akin to the zero-energy solitons at the domain wall in the Su-Schrieffer-Heeger model [50, 51, 75, 76]. Recently, it also applies in explaining the localized boundary states of high-order topological insulators [77–80]. The calculated  $\mathbb{Z}_6$  Berry phase in kagomé lattices validates the effective model in Eq. (7) in describing the ZDM in the vortex core.

To summarize, we have shown the Dirac fermions become massive in a distorted kagomé lattice of the HSD pattern induced by correlations. The existence of ZDM is further numerically confirmed, arising from the interaction with vortex potential due to the vorticity and sharing the similar mechanism with the solitons across the domain wall of Dirac mass. Finally, its topological protection is also explained by  $\mathbb{Z}_6$  Berry phase. Brief discussions on the related experiments are in order. The ZDMs in a Kekulé distorted honeycomb lattice are experimentally observed in sonic, photonic and solid-state materials[81–83], which are hopefully generalized to a distorted kagomé lattice of HSD pattern. Moreover, ultra-



cold atoms also provide a promising platform for studying interacting spinless fermions in optical kagomé lattice [84, 85]. Our findings may inspire the experimental searching for the topological phases of Dirac fermions in correlated kagomé materials.

We are indebted to Ziqiang Wang for stimulating discussions. This work is supported by Zhejiang Provincial Natural Science Foundation of China under Grant No. LZ22A040002, and National Natural Science Foundation of China under Grants No. 12174345.

---

\* Electronic address: hwachanphy@zjnu.edu.cn

- [1] Y. Wang, H. Wu, G. T. McCandless, J. Y. Chan, and M. N. Ali, *Nature Reviews Physics* **5**, 635 (2023).
- [2] S. Nishimoto, M. Nakamura, A. O'Brien, and P. Fulde, *Phys. Rev. Lett.* **104**, 196401 (2010).
- [3] A. O'Brien, F. Pollmann, and P. Fulde, *Phys. Rev. B* **81**, 235115 (2010).
- [4] A. Rüegg and G. A. Fiete, *Phys. Rev. B* **83**, 165118 (2011).
- [5] K. Ferhat and A. Ralko, *Phys. Rev. B* **89**, 155141 (2014).
- [6] L. Ye, M. Kang, J. Liu, F. von Cube, C. R. Wicker, T. Suzuki, C. Jozwiak, A. Bostwick, E. Rotenberg, D. C. Bell, L. Fu, R. Comin, and J. G. Checkelsky, *Nature* **555**, 638 (2018).
- [7] M. Kang, L. Ye, S. Fang, J.-S. You, A. Levitan, M. Han, J. I. Facio, C. Jozwiak, A. Bostwick, E. Rotenberg, M. K. Chan, R. D. McDonald, D. Graf, K. Kaznatcheev, E. Vescovo, D. C. Bell, E. Kaxiras, J. van den Brink, M. Richter, M. P. Ghimire, J. G. Checkelsky, and R. Comin, *Nature Materials* **19**, 163 (2019).
- [8] J.-X. Yin, W. Ma, T. A. Cochran, X. Xu, S. S. Zhang, H.-J. Tien, N. Shumiya, G. Cheng, K. Jiang, B. Lian, Z. Song, G. Chang, I. Belopolski, D. Multer, M. Litskevich, Z.-J. Cheng, X. P. Yang, B. Swidler, H. Zhou, H. Lin, T. Neupert, Z. Wang, N. Yao, T.-R. Chang, S. Jia, and M. Zahid Hasan, *Nature* **583**, 533 (2020).
- [9] Z. Liu, M. Li, Q. Wang, G. Wang, C. Wen, K. Jiang, X. Lu, S. Yan, Y. Huang, D. Shen, J.-X. Yin, Z. Wang, Z. Yin, H. Lei, and S. Wang, *Nature Communications* **11**, 10.1038/s41467-020-17462-4 (2020).
- [10] S. Peng, Y. Han, G. Pokharel, J. Shen, Z. Li, M. Hashimoto, D. Lu, B. R. Ortiz, Y. Luo, H. Li, M. Guo, B. Wang, S. Cui, Z. Sun, Z. Qiao, S. D. Wilson, and J. He, *Phys. Rev. Lett.* **127**, 266401 (2021).
- [11] Y. Hu, X. Wu, Y. Yang, S. Gao, N. C. Plumb, A. P. Schnyder, W. Xie, J. Ma, and M. Shi, *Science Advances* **8**, 10.1126/sciadv.add2024 (2022).
- [12] Q. Liu, H. Yao, and T. Ma, *Phys. Rev. B* **82**, 045102 (2010).
- [13] J. Wen, A. Rüegg, C.-C. J. Wang, and G. A. Fiete, *Phys. Rev. B* **82**, 075125 (2010).
- [14] W. Zhu, S.-S. Gong, T.-S. Zeng, L. Fu, and D. N. Sheng, *Phys. Rev. Lett.* **117**, 096402 (2016).
- [15] Y. Ren, T.-S. Zeng, W. Zhu, and D. N. Sheng, *Phys. Rev. B* **98**, 205146 (2018).
- [16] T.-S. Zeng, W. Zhu, and D. Sheng, *npj Quantum Materials* **3**, 10.1038/s41535-018-0120-5 (2018).
- [17] S.-L. Yu and J.-X. Li, *Phys. Rev. B* **85**, 144402 (2012).
- [18] M. L. Kiesel and R. Thomale, *Phys. Rev. B* **86**, 121105 (2012).
- [19] M. L. Kiesel, C. Platt, and R. Thomale, *Phys. Rev. Lett.* **110**, 126405 (2013).
- [20] W.-S. Wang, Z.-Z. Li, Y.-Y. Xiang, and Q.-H. Wang, *Phys. Rev. B* **87**, 115135 (2013).
- [21] X. Wu, T. Schwemmer, T. Müller, A. Consiglio, G. Sangiovanni, D. Di Sante, Y. Iqbal, W. Hanke, A. P. Schnyder, M. M. Denner, M. H. Fischer, T. Neupert, and R. Thomale, *Phys. Rev. Lett.* **127**, 177001 (2021).
- [22] X. Teng, L. Chen, F. Ye, E. Rosenberg, Z. Liu, J.-X. Yin, Y.-X. Jiang, J. S. Oh, M. Z. Hasan, K. J. Neubauer, B. Gao, Y. Xie, M. Hashimoto, D. Lu, C. Jozwiak, A. Bostwick, E. Rotenberg, R. J. Birgeneau, J.-H. Chu, M. Yi, and P. Dai, *Nature* **609**, 490 (2022).
- [23] Y. Hu, X. Wu, B. R. Ortiz, S. Ju, X. Han, J. Ma, N. C. Plumb, M. Radovic, R. Thomale, S. D. Wilson, A. P. Schnyder, and M. Shi, *Nature Communications* **13**, 10.1038/s41467-022-29828-x (2022).
- [24] M. Kang, S. Fang, J.-K. Kim, B. R. Ortiz, S. H. Ryu, J. Kim, J. Yoo, G. Sangiovanni, D. D. Sante, B.-G. Park, C. Jozwiak, A. Bostwick, E. Rotenberg, E. Kaxiras, S. D. Wilson, J.-H. Park, and R. Comin, *Nature Physics* **18**, 301 (2022).
- [25] F. Ferrari, F. Becca, and R. Valentí, *Phys. Rev. B* **106**, L081107 (2022).
- [26] Y.-Q. Liu, Y.-B. Liu, W.-S. Wang, D. Wang, and Q.-H. Wang, *Phys. Rev. B* **109**, 075127 (2024).
- [27] Z. Lin, J.-H. Choi, Q. Zhang, W. Qin, S. Yi, P. Wang, L. Li, Y. Wang, H. Zhang, Z. Sun, L. Wei, S. Zhang, T. Guo, Q. Lu, J.-H. Cho, C. Zeng, and Z. Zhang, *Phys. Rev. Lett.* **121**, 096401 (2018).
- [28] M. Kang, S. Fang, L. Ye, H. C. Po, J. Denlinger, C. Jozwiak, A. Bostwick, E. Rotenberg, E. Kaxiras, J. G. Checkelsky, and R. Comin, *Nature Communications* **11**, 10.1038/s41467-020-17465-1 (2020).
- [29] M. Li, Q. Wang, G. Wang, Z. Yuan, W. Song, R. Lou, Z. Liu, Y. Huang, Z. Liu, H. Lei, Z. Yin, and S. Wang, *Nature Communications* **12**, 10.1038/s41467-021-23536-8 (2021).
- [30] S. Regmi, T. Fernando, Y. Zhao, A. P. Sakhya, G. Dhakal, I. Bin Elius, H. Vazquez, J. D. Denlinger, J. Yang, J.-H. Chu, X. Xu, T. Cao, and M. Neupane, *Communications Materials* **3**, 10.1038/s43246-022-00318-3 (2022).
- [31] Z. Sun, H. Zhou, C. Wang, S. Kumar, D. Geng, S. Yue, X. Han, Y. Haraguchi, K. Shimada, P. Cheng, L. Chen, Y. Shi, K. Wu, S. Meng, and B. Feng, *Nano Letters* **22**, 4596 (2022).
- [32] Y. Hu, S. M. Teicher, B. R. Ortiz, Y. Luo, S. Peng, L. Huai, J. Ma, N. C. Plumb, S. D. Wilson, J. He, and M. Shi, *Science Bulletin* **67**, 495 (2022).
- [33] S. Gao, S. Zhang, C. Wang, S. Yan, X. Han, X. Ji, W. Tao, J. Liu, T. Wang, S. Yuan, G. Qu, Z. Chen, Y. Zhang, J. Huang, M. Pan, S. Peng, Y. Hu, H. Li, Y. Huang, H. Zhou, S. Meng, L. Yang, Z. Wang, Y. Yao, Z. Chen, M. Shi, H. Ding, H. Yang, K. Jiang, Y. Li, H. Lei, Y. Shi, H. Weng, and T. Qian, *Phys. Rev. X* **13**, 041049 (2023).
- [34] S.-Q. Shen, *Topological Insulators* (Springer Singapore, 2017).
- [35] B. A. Bernevig and T. L. Hughes, *Topological Insulators and Topological Superconductors*.

- (Princeton University Press, Princeton, 2013).
- [36] C. L. Kane and E. J. Mele, *Phys. Rev. Lett.* **95**, 226801 (2005).
- [37] C. L. Kane and E. J. Mele, *Phys. Rev. Lett.* **95**, 146802 (2005).
- [38] H.-M. Guo and M. Franz, *Phys. Rev. B* **80**, 113102 (2009).
- [39] Z.-Y. Zhang, *Journal of Physics: Condensed Matter* **23**, 365801 (2011).
- [40] A. Bolens and N. Nagaosa, *Phys. Rev. B* **99**, 165141 (2019).
- [41] G. Xu, B. Lian, and S.-C. Zhang, *Phys. Rev. Lett.* **115**, 186802 (2015).
- [42] M. Ezawa, *Phys. Rev. Lett.* **120**, 026801 (2018).
- [43] X. Lu, Y. Chen, and H. Chen, *Phys. Rev. B* **101**, 195143 (2020).
- [44] A. Sil and A. K. Ghosh, *Journal of Physics: Condensed Matter* **32**, 205601 (2020).
- [45] M. A. J. Herrera, S. N. Kempkes, M. B. de Paz, A. García-Etxarri, I. Swart, C. M. Smith, and D. Bercioux, *Phys. Rev. B* **105**, 085411 (2022).
- [46] H. Zhou, H. Liu, H. Ji, X. Li, S. Meng, and J.-T. Sun, *npj Quantum Materials* **8**, 10.1038/s41535-023-00548-9 (2023).
- [47] H. Xue, Y. Yang, F. Gao, Y. Chong, and B. Zhang, *Nature Materials* **18**, 108 (2018).
- [48] M. Li, D. Zhirihin, M. Gorchak, X. Ni, D. Filonov, A. Slobozhanyuk, A. Alù, and A. B. Khanikaev, *Nature Photonics* **14**, 89 (2019).
- [49] A. El Hassan, F. K. Kunst, A. Moritz, G. A. Andler, E. J. Bergholtz, and M. Bourennane, *Nature Photonics* **13**, 697 (2019).
- [50] R. Jackiw and C. Rebbi, *Phys. Rev. D* **13**, 3398 (1976).
- [51] W. P. Su, J. R. Schrieffer, and A. J. Heeger, *Phys. Rev. Lett.* **42**, 1698 (1979).
- [52] R. Jackiw and P. Rossi, *Nuclear Physics B* **190**, 681 (1981).
- [53] N. Read and D. Green, *Phys. Rev. B* **61**, 10267 (2000).
- [54] C.-Y. Hou, C. Chamon, and C. Mudry, *Phys. Rev. Lett.* **98**, 186809 (2007).
- [55] R. Jackiw and S.-Y. Pi, *Phys. Rev. Lett.* **98**, 266402 (2007).
- [56] C. Chamon, C.-Y. Hou, R. Jackiw, C. Mudry, S.-Y. Pi, and G. Semenoff, *Phys. Rev. B* **77**, 235431 (2008).
- [57] F. Wilczek, *Phys. Rev. Lett.* **49**, 957 (1982).
- [58] F. Wilczek and A. Zee, *Phys. Rev. Lett.* **51**, 2250 (1983).
- [59] B. Seradjeh and M. Franz, *Phys. Rev. Lett.* **101**, 146401 (2008).
- [60] M. Greiter and F. Wilczek, *Annual Review of Condensed Matter Physics* **15**, 131 (2024).
- [61] Y.-X. Jiang, J.-X. Yin, M. M. Denner, N. Shumiya, B. R. Ortiz, G. Xu, Z. Guguchia, J. He, M. S. Hossain, X. Liu, J. Ruff, L. Kautzsch, S. S. Zhang, G. Chang, I. Belopolski, Q. Zhang, T. A. Cochran, D. Multer, M. Litskevich, Z.-J. Cheng, X. P. Yang, Z. Wang, R. Thomale, T. Neupert, S. D. Wilson, and M. Z. Hasan, *Nature Materials* **20**, 1353 (2021).
- [62] H. Tan, Y. Liu, Z. Wang, and B. Yan, *Phys. Rev. Lett.* **127**, 046401 (2021).
- [63] L. Fu and C. L. Kane, *Phys. Rev. Lett.* **100**, 096407 (2008).
- [64] H. W. S. Arachchige, W. R. Meier, M. Marshall, T. Matsuoka, R. Xue, M. A. McGuire, R. P. Hermann, H. Cao, and D. Mandrus, *Phys. Rev. Lett.* **129**, 216402 (2022).
- [65] T. Hu, H. Pi, S. Xu, L. Yue, Q. Wu, Q. Liu, S. Zhang, X. Li, X. Zhou, J. Yuan, D. Wu, T. Dong, H. Weng, and N. Wang, *Phys. Rev. B* **107**, 165119 (2023).
- [66] J. Kang and O. Vafek, *Phys. Rev. Lett.* **122**, 246401 (2019).
- [67] K. Seo, V. N. Kotov, and B. Uchoa, *Phys. Rev. Lett.* **122**, 246402 (2019).
- [68] N. Bultinck, E. Khalaf, S. Liu, S. Chatterjee, A. Vishwanath, and M. P. Zaletel, *Phys. Rev. X* **10**, 031034 (2020).
- [69] B. A. Bernevig, Z.-D. Song, N. Regnault, and B. Lian, *Phys. Rev. B* **103**, 205413 (2021).
- [70] X. Feng, K. Jiang, Z. Wang, and J. Hu, *Science Bulletin* **66**, 1384 (2021).
- [71] J.-W. Dong, Z. Wang, and S. Zhou, *Phys. Rev. B* **107**, 045127 (2023).
- [72] F. m. c. Gygi and M. Schlüter, *Phys. Rev. B* **43**, 7609 (1991).
- [73] A. De Martino, L. Dell'Anna, and R. Egger, *Phys. Rev. Lett.* **98**, 066802 (2007).
- [74] Y. Hatsugai and I. Maruyama, *EPL (Europhysics Letters)* **95**, 20003 (2011).
- [75] W. P. Su, J. R. Schrieffer, and A. J. Heeger, *Phys. Rev. B* **22**, 2099 (1980).
- [76] A. Niemi and G. Semenoff, *Physics Reports* **135**, 99 (1986).
- [77] W. A. Benalcazar, B. A. Bernevig, and T. L. Hughes, *Science* **357**, 61 (2017).
- [78] W. A. Benalcazar, B. A. Bernevig, and T. L. Hughes, *Phys. Rev. B* **96**, 245115 (2017).
- [79] Z. Song, Z. Fang, and C. Fang, *Phys. Rev. Lett.* **119**, 246402 (2017).
- [80] F. Schindler, A. M. Cook, M. G. Vergniory, Z. Wang, S. S. P. Parkin, B. A. Bernevig, and T. Neupert, *Science Advances* **4**, 10.1126/sciadv.aat0346 (2018).
- [81] P. Gao, D. Torrent, F. Cervera, P. San-Jose, J. Sánchez-Dehesa, and J. Christensen, *Phys. Rev. Lett.* **123**, 196601 (2019).
- [82] A. J. Menssen, J. Guan, D. Felce, M. J. Booth, and I. A. Walmsley, *Phys. Rev. Lett.* **125**, 117401 (2020).
- [83] Y. Guan, C. Dutreix, H. González-Herrero, M. M. Ugeda, I. Brihuega, M. I. Katsnelson, O. V. Yazyev, and V. T. Renard, *Nature Communications* **15**, 10.1038/s41467-024-47267-8 (2024).
- [84] G.-B. Jo, J. Guzman, C. K. Thomas, P. Houser, A. Vishwanath, and D. M. Stamper-Kurn, *Phys. Rev. Lett.* **108**, 045305 (2012).
- [85] D. Yamamoto, C. Sato, T. Nikuni, and S. Tsuchiya, *Phys. Rev. Lett.* **110**, 145304 (2013).